CRITICAL AND COMPENSATION BEHAVIORS OF A HEXAGONAL ISING NANOTUBE WITH NEGATIVE CORE-SHELL COUPLING

OUAFA HACHEM[1], AMER LAFHAL[1,2,*], EL MOSTAFA JALAL[1,3], ABDELMOUMEN EL ANTARI[1], MOHAMMED EL BOUZIANI[1]

[1]Theoretical Physics Team, Laboratory L.P.M.C., Faculty of Sciences, Chouaib Doukkali University, El Jadida, Morocco
[2]Chouaib Doukkali University, Higher School of Education and Training (ESEF), El Jadida, Morocco
Corresponding author*: lafhal.a@ucd.ac.ma
[3]LS2ME Laboratory, Polydisciplinary Faculty of Khouribga, Sultan Moulay Slimane University, Beni Mellal, Morocco

Received February 26, 2023

Abstract. The mean field approximation has been used to study a ferrimagnetic hexagonal Ising nanotube consisting of a spin-1/2 core surrounded by a spin-1 shell with negative core-shell exchange coupling. More precisely, we have investigated the effects of the crystal field, the shell exchange coupling and the core-shell interfacial exchange coupling on the magnetic properties and phase diagrams of the system. The critical and compensation behaviors are highlighted for appropriate values of the Hamiltonian parameters, as well as the first-order phase transition in the ferrimagnetic ordered region at low temperatures.

Key words: Core-Shell Nanotube; Mean field; Phase diagram; Compensation.

1. INTRODUCTION

Over the past few years, the studies on magnetic nanostructures such as nanotubes, nanowires, nanoparticles and nanofilms have aroused considerable interest on the part of many researchers. This is due to their particular properties in comparison with bulk materials like the increasing surface-volume ratio and the small size of the particles, which leads to the dominance of surface atoms over those inside and the emergence of domains characterized by quantum effects [1–3]. A further reason is that the nanostructured systems have several technological potential uses in various fields, for example, they can be used for sensors [4], optoelectronic devices [5, 6], energy storage [7], biomedicine and biotechnology [8, 9]. The properties of nanostructures are not only dependent on their sizes, but they are also related to their shapes: cube, prism, hexagon, octahedron, disk, rod, wire, tube, etc. [1]. However, the magnetic nanomaterials can be synthesized in multiple structures, but the core-shell one is the most suitable to exhibit excellent performances [1, 10]. Generally, the core-shell model is used to explain certain characteristic behaviors of magnetic nanostructures.

On the other hand, ferrimagnets such as iron garnets, hexaferrites, spinel ferrites and rare-earth/iron intermetallic compounds are among the most interesting magnetic materials due to their particular properties [11]. They consist of two or more sublattices with inequivalent moments interacting antiferromagnetically. Under certain circumstances, the sublattices magnetizations compensate each other, and thus the total magnetization is cancelled at a temperature called the compensation temperature (T_{comp}) lower than the critical temperature (T_C) [12]. The phenomenon of compensation is technologically very useful in various fields such as magneto-optical recording [13] and magnetic information storage [14]. In addition, ferrimagnets are protected against external magnetic disturbances as they react less well to magnetic fields [14].

Theoretically, there are several studies devoted to core-shell nanosystems; among them, we find Ising nanostructures with spin-1/2 in the core and spin-1 in the surface shell. Zaim *et al.* [15, 16] have used the Monte Carlo simulation (MCS) to study the critical behaviors and magnetic properties of a nanocube [15] and a spherical nanoparticle [16], and they have obtained some very important results, especially the multi-compensation behavior and the influences of the shell coupling and the core-shell interfacial coupling on the critical and compensation temperatures. Canko *et al.* [17] have investigated a cylindrical Ising nanotube using effective field theory (EFT), and they have found both first- and second-order phase transitions, as well as critical and tricritical points. The critical and compensation behaviors of a ferrimagnetic cylindrical Ising nanowire have been studied by Boughrara *et al.* using MCS and EFT [18]; this system shows very rich critical phenomena, including first- and second-order transitions, tricritical behavior and critical end-point. Also, Mendes *et al.* [19, 20] have used the mean field approximation (MFA) to examine the thermodynamic states of a hexagonal nanotube [19] and a hexagonal nanowire [20], where the first- and second-order phase transitions are observed, and the stable, metastable and unstable states are found and classified. Recently, Deviren [21] has examined the nonequilibrium magnetic properties and hysteresis loops for the kinetic mixed-spin (1/2, 1) Ising nanowire by the Glauber-type stochastic dynamics; the dynamic phase diagrams present paramagnetic, ferrimagnetic and nonmagnetic phases, reentrant phenomena and dynamic tricritical points.

The aim of this paper is to use the mean field approach for studying the phase diagrams and magnetic properties of a hexagonal Ising nanotube consisting of spin-1/2 core and spin-1 shell with negative core-shell exchange coupling. Thus, our present research can be seen as a continuation of the works mentioned above, especially that carried out by Canko *et al.* [17], which studied a nanotube having a structure similar to ours. The outline of the remaining part of this work is as follows: in Section 2, we present the basic concepts of our studied model and we give briefly the formulation of the MFA method. The results and discussions are shown

in Section 3. Finally, Section 4 is dedicated to a conclusion.

2. MODEL AND METHOD

In this work, we investigate a ferrimagnetic hexagonal core-shell nanotube within the Ising model, composed of a spin-1/2 ferromagnetic core wrapped by a spin-1 ferromagnetic shell (Fig. 1), and described by the following Hamiltonian:

$$H = -J_C \sum_{\langle ij \rangle} \sigma_i \sigma_j - J_S \sum_{\langle kl \rangle} S_k S_l - J_{int} \sum_{\langle ik \rangle} \sigma_i S_k - D_S \sum_{k=1}^{12N} S_k^2 \qquad (1)$$

where the core sites are filled with spins σ taking values of $\pm 1/2$, whereas the shell sites are filled with spins S taking values of 0 and ± 1. J_S and J_C are positive exchange couplings between two nearest neighboring spins, respectively, in the surface shell and in the core. J_{int} is a negative core-shell interfacial exchange coupling between two nearest neighboring spins, one in the shell and the other in the core. D_S denotes the crystal field applied to the surface shell sublattice. The total number of spins in the nanotube is $N_T = N_S + N_C = 18N$ with $N_S = 12N$ and $N_C = 6N$ are the numbers of spins in the shell and in the core respectively, and N is the number of hexagonal layers [22]. In this study, we consider the coupling J_C as a unit of energy.

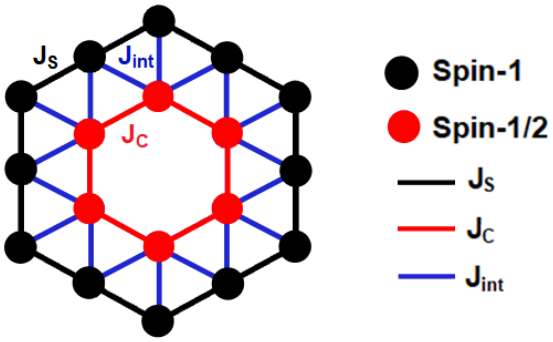

Fig. 1 – Cross-section of a hexagonal nanotube constituted of core spins $\sigma = 1/2$ and shell spins $S = 1$.

To examine this nanotube by MFA, we rely on Bogoliubov's variational principle for the free energy [23]:

$$F(H) \leq -\frac{1}{\beta} \ln(Z_0) + \langle H - H_0 \rangle_0 \equiv \Phi \qquad (2)$$

where $F(H)$ is the free energy of the Hamiltonian H presented in Eq. (1), H_0 is an effective Hamiltonian dependent on variational parameters, and $\langle H - H_0 \rangle_0$ is the average value over the ensemble defined by H_0. Z_0 is the partition function

generated by the Hamiltonian H_0 and defined as follows: $Z_0 = Tr\left(\exp\left(-\beta H_0\right)\right)$ with $\beta = 1/k_B T$ (k_B is the Boltzmann constant and T is the absolute temperature; we take $k_B = 1$ in order to simplify the calculations).

We consider here a simpler form of the effective Hamiltonian:

$$H_0 = -\alpha_\sigma \sum_{i=1}^{6N} \sigma_i - \alpha_{S_1} \sum_{k=1}^{6N} S_k - D_S \sum_{k=1}^{6N} S_k^2 - \alpha_{S_2} \sum_{l=1}^{6N} S_l - D_S \sum_{l=1}^{6N} S_l^2 \qquad (3)$$

where α_σ is a variational parameter related to the core spins $\sigma = 1/2$, and α_{S_1} and α_{S_2} are two variational parameters related to the shell spins $S = 1$, respectively, in the corners and in the midpoints of the sides of the shell layers.

This nanotube is divided into three sublattices: (L_σ), (L_{S_1}) and (L_{S_2}). (L_σ) consists of spins $\sigma = 1/2$ in the core, while (L_{S_1}) and (L_{S_2}) are composed of spins $S = 1$ situated, respectively, in the corners and in the midpoints of the sides of the shell layers.

Thus, the expression of the approximate energy Φ can be easily obtained in the following form:

$$\Phi = 6N \begin{pmatrix} -\frac{1}{\beta}\ln\left[2\cosh\left(\frac{1}{2}\beta\alpha_\sigma\right)\right] - \frac{1}{\beta}\ln\left[1+2\exp\left(\beta D_S\right)\cosh\left(\beta\alpha_{S_1}\right)\right] \\ -\frac{1}{\beta}\ln\left[1+2\exp\left(\beta D_S\right)\cosh\left(\beta\alpha_{S_2}\right)\right] + \alpha_\sigma m_C + \alpha_{S_1} m_{S_1} + \alpha_{S_2} m_{S_2} \\ -2J_C m_C^2 - J_S m_{S_1}^2 - J_S m_{S_2}^2 - 2J_S m_{S_1} m_{S_2} - J_{int} m_C m_{S_1} \\ -2J_{int} m_C m_{S_2} \end{pmatrix} \qquad (4)$$

where $m_C = \langle\sigma_i\rangle$, $m_{S_1} = \langle S_k\rangle$ and $m_{S_2} = \langle S_l\rangle$ are the magnetizations per site of the sublattices (L_σ), (L_{S_1}) and (L_{S_2}) respectively.

Through the minimization of the energy Φ depending on the variational parameters, the mean field equations can be written as follows:

$$\begin{cases} m_C = \frac{1}{2}\tanh\left(\frac{1}{2}\beta\alpha_\sigma\right) \\ m_{S_1} = \frac{2\exp(\beta D_S)\sinh\left(\beta\alpha_{S_1}\right)}{1+2\exp(\beta D_S)\cosh\left(\beta\alpha_{S_1}\right)} \\ m_{S_2} = \frac{2\exp(\beta D_S)\sinh\left(\beta\alpha_{S_2}\right)}{1+2\exp(\beta D_S)\cosh\left(\beta\alpha_{S_2}\right)} \end{cases} \qquad (5)$$

where:

$$\begin{cases} \alpha_\sigma = 4J_C m_C + J_{int} m_{S_1} + 2J_{int} m_{S_2} \\ \alpha_{S_1} = J_{int} m_C + 2J_S m_{S_1} + 2J_S m_{S_2} \\ \alpha_{S_2} = 2J_{int} m_C + 2J_S m_{S_1} + 2J_S m_{S_2} \end{cases} \qquad (6)$$

Then, the shell magnetization per site (m_S) and the total magnetization per site (M_T) are calculated as follows:

$$m_S = \frac{m_{S_1} + m_{S_2}}{2} \qquad \text{and} \qquad M_T = \frac{6\, m_C + 12\, m_S}{18} \qquad (7)$$

The mean field equations (5) are self-consistent equations, which will be solved

numerically. In general, the solutions of these equations depend on the initial values of the magnetizations m_C, m_{S_1} and m_{S_2}; the solution taken into account and presenting the stable equilibrium phase is that which minimizes the free energy. Additionally, the critical temperature (T_C) exhibiting second-order phase transition is determined when the magnetizations are continuous near $m_S = m_C = M_T = 0$, whilst the first-order transition temperature is described by discontinuities in these magnetizations.

For appropriate physical parameters, and since we have considered a negative core-shell interfacial exchange coupling ($J_{int} < 0$), the core and shell magnetizations can be different from zero ($m_C < 0$ and $m_S > 0$) in an ordered ferrimagnetic phase so that $M_T = 0$. The corresponding temperature in this case is called the compensation temperature (T_{comp}), which is lower than the critical temperature ($T_{comp} < T_C$), such that:

$$m_C\left(T_{comp}\right) = -2 \times m_S\left(T_{comp}\right) \qquad \text{and} \qquad M_T\left(T_{comp}\right) = 0 \tag{8}$$

Finally, the determination of the critical, first-order and compensation temperatures allows us to plot the phase diagrams.

3. RESULTS AND DISCUSSION

In this section, we investigate and discuss the influences of the crystal field (D_S), the shell exchange coupling (J_S) and the core-shell interfacial exchange coupling (J_{int}) on the magnetizations and phase diagrams of our hexagonal nanotube using the MFA. We will show certain typical phase diagrams and certain magnetization curves for selected values of the Hamiltonian parameters.

3.1. EFFECT OF THE CRYSTAL FIELD

First, the influence of the crystal field interaction D_S on the magnetic properties of the system is highlighted in Figs. 2 and 3. Figure 2 exhibits the thermal variations of the sublattice magnetizations m_C and m_S in (a) and the total magnetization M_T in (b) for some selected values of D_S/J_C when $J_S/J_C = 0.5$ and $J_{int}/J_C = -0.1$. From Fig. 2(a), it is observed that for $D_S/J_C > -1.038$ as for $D_S/J_C = -1$ and 0, the magnetizations m_C and m_S begin from their saturation values -0.5 and 1 respectively at $T = 0$, and vary (m_C increases and m_S decreases) continuously until vanishing beyond the critical temperature (T_C). This justifies that there is only second-order phase transition for these values of D_S/J_C. In the interval $-1.075 \leq D_S/J_C \leq -1.038$, m_S shows a discontinuous jump at low temperature followed by continuous variation until it cancels out at T_C, which means the existence of first-order phase transition followed by another of second-order. We can also say

that the stable ferrimagnetic phase in the domain $D_S/J_C \geq -1.075$ is ($m_C = -1/2$, $m_S = 1$). For $D_S/J_C < -1.075$ as for $D_S/J_C = -3$ and -1.2, m_C and m_S start from the initial values -0.5 and 0 respectively at $T = 0$ and vary in a continuous way to zero at T_C; the stable ferrimagnetic phase in this domain is ($m_C = -1/2$, $m_S = 0$) and the system shows only second-order transition.

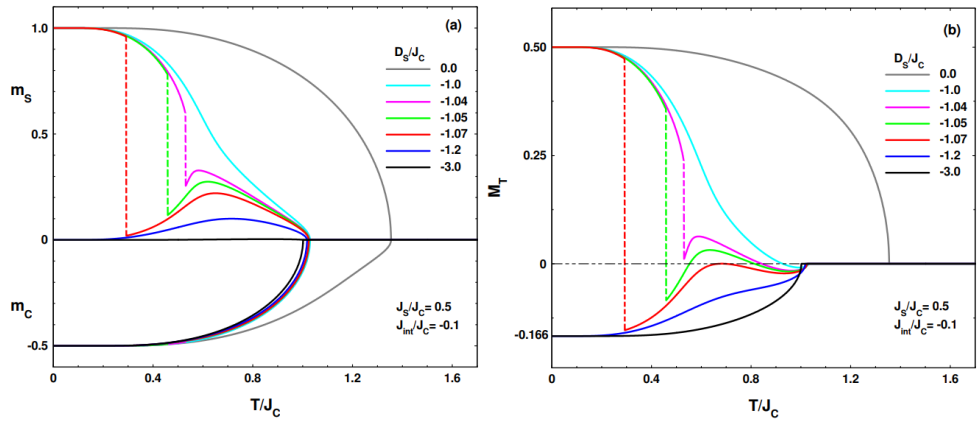

Fig. 2 – The magnetizations m_S and m_C (a) and M_T (b) as a function of temperature for some selected values of D_S/J_C when $J_S/J_C = 0.5$ and $J_{int}/J_C = -0.1$.

From Fig. 2(b), it is mentioned that the saturation value of the total magnetization M_T takes one of the two following values: -0.166 for $D_S/J_C < -1.075$ and 0.5 for $D_S/J_C \geq -1.075$. We also notice the appearance of the compensation behavior; there are two compensation points (T_{comp}) in the range $-1.07 \leq D_S/J_C \leq -1.041$, and one compensation point in the range $-1.04 \leq D_S/J_C \leq -0.93$. Moreover, the discontinuous jumps observed in the M_T curves for $D_S/J_C = -1.07$, -1.05 and -1.04 justify the presence of first-order transition for $-1.075 \leq DS/JC \leq -1.038$.

Figure 3 shows a typical phase diagram in the (D_S/J_C, T/J_C) plane when $J_S/J_C = 0.5$ and $J_{int}/J_C = -0.1$. From this figure, we can see the existence of first- and second-order phase transition lines. The critical temperature representing second-order transition is constant ($T_C/J_C = 1.0$) for all values of D_S/J_C less than -1.5, and then increases with the increase of D_S/J_C until reaching a saturation value for large positive values of crystal field. Furthermore, a first-order transition line separating the two ferrimagnetic phases ($m_C = -1/2$, $m_S = 0$) and ($m_C = -1/2$, $m_S = 1$) exists in the ordered region at low temperatures, starting from ($T/J_C = 0$, $D_S/J_C = -1.075$) and ending at a critical point connected to the compensation line. The coordinates of this last point are ($T/J_C = 0.546$, $D_S/J_C = -1.038$). It is also noted that the line connecting the compensation points begins from the end of the first-order line and extends to meet the second-order one. Our results obtained here

for the crystal field effect can be compared with those found in certain ferrimagnetic nanostructured Ising systems [17, 18, 24–28]. Phase diagrams similar to our diagram were obtained by the use of MCS for hexagonal nanowires with core-shell morphology and mixed spins (1/2, 1) [18] and (3/2, 1) [24], for a hexagonal nanowire with alternate layers of spins $S = 3/2$ and $S = 1$ [25], and for mixed-spin (1, 3/2) system [26]. However, the profile of these diagrams without first-order transition has already been encountered in numerical simulations of certain nanosystems such as a mixed spin-3/2 and spin-1 bilayer superlattice system [27] and a cubic nanoparticle with spin-1/2 core and spin-3/2 shell [28]. Eventually, it should be mentioned that the work studying this same nanotube *via* EFT [17] have found a phase diagram in the (crystal field, temperature) plane similar to ours but without compensation temperatures.

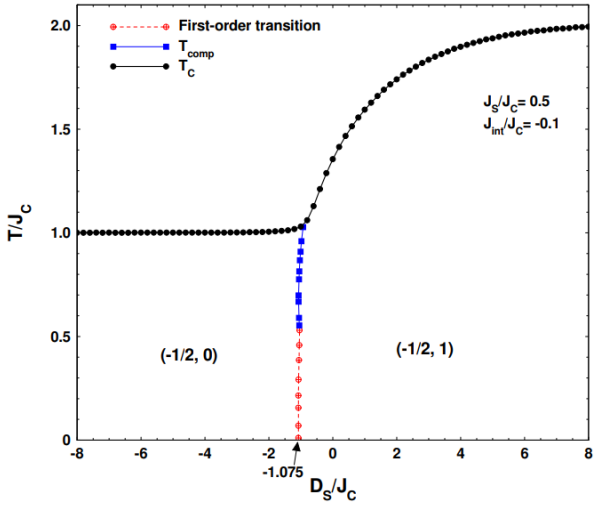

Fig. 3 – The phase diagram in the $(D_S/J_C, T/J_C)$ plane when $J_S/J_C = 0.5$ and $J_{int}/J_C = -0.1$.

3.2. EFFECT OF THE SHELL EXCHANGE COUPLING

We now examine the influence of the shell exchange coupling J_S on the magnetizations and phase diagrams of the nanotube in Figs. 4 and 5. We start by presenting the thermal variations of the magnetizations m_C, m_S (a) and M_T (b) in Fig. 4 for certain chosen values of J_S/J_C when $D_S/J_C = 1$ and $J_{int}/J_C = -0.1$. From this figure, it can be observed that the magnetizations m_C, m_S and M_T show the following saturation values: -0.5, 1 and 0.5 respectively, whatever the value of J_S/J_C; this indicates that the stable ferrimagnetic phase at low temperatures is ($m_C = -1/2$, $m_S = 1$). Moreover, m_S decreases and m_C increases continuously from their saturation values until they cancel out beyond T_C; there is only a second-order phase

transition regardless of the value of J_S/J_C. In the range $0 \leq J_S/J_C \leq 0.23$, the M_T curves exhibit a single point of compensation as for $J_S/J_C = 0$, 0.1 and 0.2 in Fig. 4(b). Finally, there are three types of M_T curves based on Néel's classification: Q-, P- and N-type [12, 29].

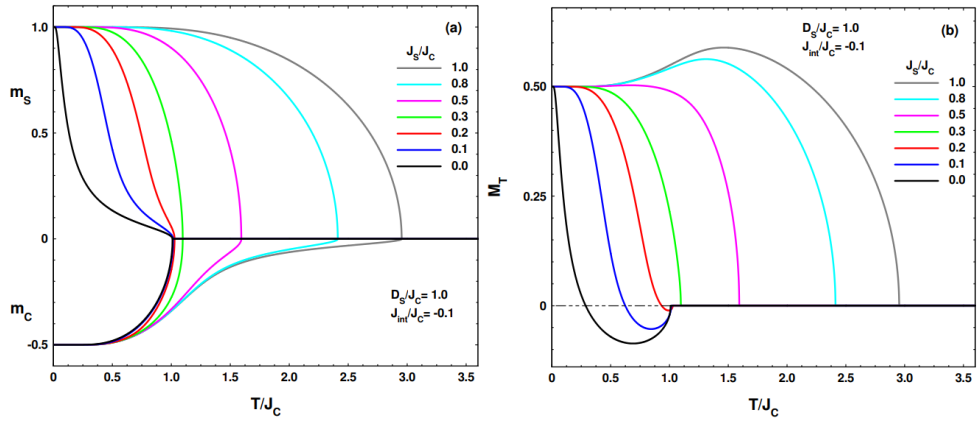

Fig. 4 – The magnetizations m_S and m_C (a) and M_T (b) as a function of temperature for some selected values of J_S/J_C when $D_S/J_C = 1.0$ and $J_{int}/J_C = -0.1$.

In Fig. 5, a typical phase diagram is plotted in the (J_S/J_C, T/J_C) plane for $J_{int}/J_C = -0.1$ and $D_S/J_C = 1$. In this diagram, a second-order phase transition separates the ferrimagnetic phase ($m_C = -1/2$, $m_S = 1$) at low temperatures from the paramagnetic phase at high temperatures. The critical temperature remains constant ($T_C/J_C = 1.01$) for small values of J_S/J_C, and then increases linearly as J_S/J_C increases. Furthermore, the compensation behavior appear only for weak shell exchange interactions, in particular for $0 \leq J_S/J_C \leq 0.23$, and T_{comp} increases with the increase of J_S/J_C. It is noteworthy to mention that our phase diagram obtained in Fig. 5 is in qualitative agreement with others plotted using MCS and EFT in some studies of magnetic nanostructures with core-shell structure such as nanotubes [30, 31], nanowires [18, 31–34], nanoparticles [16, 28] and nanocubes [15]. Moreover, in previous works where we have used MFA [35] and MCS [36] to investigate a hexagonal nanotube with spin-1/2 in the core and spin-3/2 in the shell, we have found a similar diagram in the (J_S/J_C, T/J_C) plane but with the presence of a first-order transition line at low temperature in the ferrimagnetic ordered region.

3.3. EFFECT OF THE CORE-SHELL INTERFACIAL EXCHANGE COUPLING

In this last subsection, the effect of the core-shell interfacial exchange coupling J_{int} on the magnetic properties of our nanotube is studied in Figs. 6 and 7. The magnetizations m_C, m_S (a) and M_T (b) as a function of T/J_C are presented in Fig.

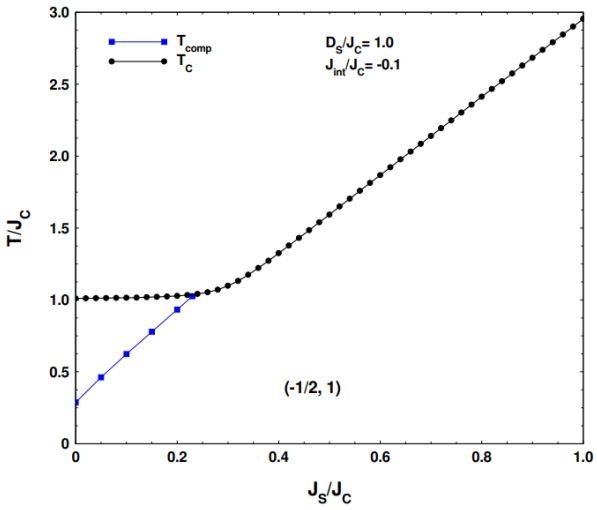

Fig. 5 – The phase diagram in the $(J_S/J_C, T/J_C)$ plane when $D_S/J_C = 1.0$ and $J_{int}/J_C = -0.1$.

6 for selected values of J_{int}/J_C when $J_S/J_C = 0.1$ and $D_S/J_C = 1$. It can be seen here that the magnetizations m_C, m_S and M_T vary gradually from their initial values -0.5, 1 and 0.5 respectively up to T_C where they vanish. Note also that m_S decreases asymptotically to zero for $J_{int}/J_C = -0.01$. In the range $-0.32 \leq J_{int}/J_C < 0$ as for $J_{int}/J_C = -0.01$, -0.15 and -0.3 in Fig. 6(b), there is the existence of a single point of compensation.

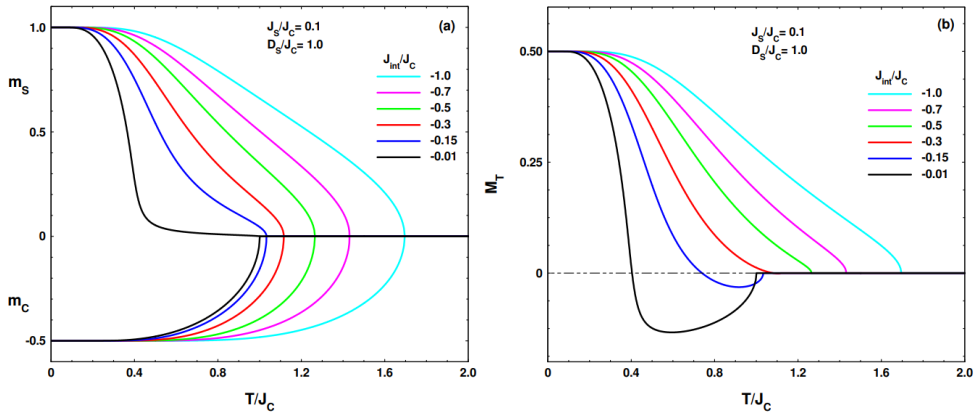

Fig. 6 – The magnetizations m_S and m_C (a) and M_T (b) as a function of temperature for some selected values of J_{int}/J_C when $J_S/J_C = 0.1$ and $D_S/J_C = 1.0$.

Figure 7 displays a typical phase diagram in the $(J_{int}/J_C, T/J_C)$ plane obtained when $J_S/J_C = 0.1$ and $D_S/J_C = 1$. This diagram resembles the one plotted

in the (J_S/J_C, T/J_C) plane in Fig. 5; there is also here a second-order transition between the ferrimagnetic and paramagnetic phases, but the discord lies in the absence of a constant critical temperature for weak values of J_{int}/J_C. In addition, since we have considered the ferrimagnetic case ($J_{int} < 0$), this favored the appearance of compensation temperatures in particular for small values of J_{int}; T_{comp} is observed in the domain $-0.32 \leq J_{int}/J_C < 0$. We notice that T_C and T_{comp} increase with decreasing J_{int}/J_C. For comparison, it should be noted that similar phase diagrams in the (J_{int}, temperature) plane have been plotted in some works investigating core-shell Ising nanosystems [15, 16, 18, 30–36].

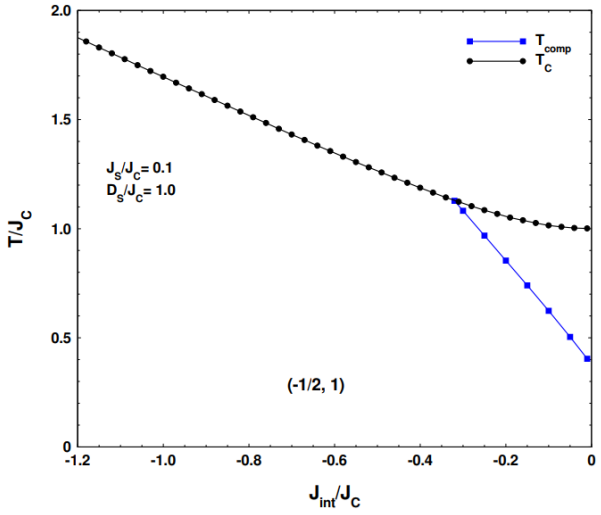

Fig. 7 – The phase diagram in the (J_{int}/J_C, T/J_C) plane when $J_S/J_C = 0.1$ and $D_S/J_C = 1.0$.

Finally, as we can see in this study by the use of the mean field approximation, the interactions (J_S, J_{int} and D_S) and the temperature have influences on the phase diagrams and magnetic properties of the nanotube. For some values of these parameters, the system can show important results, in particular two ordered ferrimagnetic phases separated by a low temperature first-order transition, second-order phase transitions and compensation behavior for weak exchange interactions.

4. CONCLUSION

In summary, the phase diagrams and magnetic properties of a ferrimagnetic hexagonal Ising nanotube with spin-1/2 core and spin-1 shell have been studied using mean field approximation. We have examined the effects of the crystal field, the shell exchange coupling and the core-shell interfacial exchange coupling on the critical and compensation behaviors of the system. According to certain values of the

Hamiltonian parameters, typical phase diagrams are plotted in three planes, where the system can show very rich results including second-order phase transitions and compensation temperatures. In the (crystal field, temperature) plane, there is the appearance of two ferrimagnetic phases ($m_C = -1/2$, $m_S = 0$) and ($m_C = -1/2$, $m_S = 1$) separated by a first-order transition line at low temperatures ending at a critical point. Concerning the compensation behavior, it always appears for small values of exchange couplings (J_S and J_{int}).

REFERENCES

1. R.G. Chaudhuri, S. Paria, Chem. Rev. 112, 2373 (2012).
2. R.K. Goyal, *Nanomaterials and Nanocomposites: Synthesis, Properties, Characterization Techniques, and Applications*, CRC Press, Boca Raton, USA, (2018).
3. B. Rogers, J. Adams, S. Pennathur, *Nanotechnology: Understanding Small Systems*, CRC Press, Boca Raton, USA, (2015).
4. E. Bagheri, L. Ansari, E. Sameiyan, K. Abnous, S.M. Taghdisi, M. Ramezani, M. Alibolandi, Biosens. Bioelectron. 153, 112054 (2020).
5. V.V. Ursaki, S. Lehmann, V.V. Zalamai, V. Morari, K. Nielsch, I.M. Tiginyanu, E.V. Monaico, Rom. J. Phys. 68, 601 (2023).
6. G.M. Kumar, P. Ilanchezhiyan, H.D. Cho, S. Yuldashev, H.C. Jeon, D.Y. Kim, T.W. Kang, Nanomaterials 9, 924 (2019).
7. M.F.L. De Volder, S.H. Tawfick, R.H. Baughman, A.J. Hart, Science 339, 535 (2013).
8. L. Peixoto, R. Magalhães, D. Navas, S. Moraes, C. Redondo, R. Morales, J.P. Araújo, C.T. Sousa, Appl. Phys. Rev. 7, 011310 (2020).
9. E.G. Chronopoulou, E. Ioannou, F. Perperopoulou, N.E. Labrou, *"Protein Nanostructures with Purpose-Designed Properties in Biotechnology and Medicine", pp 71-89, In: P. Shukla (eds) Microbial Enzymes and Biotechniques*, Springer, Singapore, (2020).
10. H. Zheng, T. Zhai, M. Yu, S. Xie, C. Liang, W. Zhao, S.C.I. Wang, Z. Zhang, X. Lu, J. Mater. Chem. C 1, 225 (2013).
11. K.P. Belov, Phys-Usp. 39, 623 (1996).
12. L. Néel, Ann. Phys. 12, 137 (1948).
13. S. Tsunashima, J. Phys. D: Appl. Phys. 34, R87 (2001).
14. J. Finley, L. Liu, Appl. Phys. Lett. 116, 110501 (2020).
15. A. Zaim, M. Kerouad, Y. El Amraoui, J. Magn. Magn. Mater. 321, 1077 (2009).
16. A. Zaim, M. Kerouad, Physica A 389, 3435 (2010).
17. O. Canko, A. Erdinç, F. Taşkın, A.F. Yıldırım, J. Magn. Magn. Mater. 324, 508 (2012).
18. M. Boughrara, M. Kerouad, A. Zaim, J. Magn. Magn. Mater. 360, 222 (2014).
19. R.G.B. Mendes, F.C. Sá Barreto, J.P. Santos, Physica A 505, 1186 (2018).
20. R.G.B. Mendes, F.C. Sá Barreto, J.P. Santos, Braz. J. Phys. 48, 137 (2018).
21. B. Deviren, Physica E 120, 114052 (2020).
22. N. Hachem, Y. Al Qahoom, R. Aharrouch, M. Madani, M. El Bouziani, Rom. J. Phys. 67, 612 (2022).
23. H. Falk, Am. J. Phys. 38, 858 (1970).
24. A. Feraoun, A. Zaim, M. Kerouad, Physica B 445, 74 (2014).

25. A. Feraoun, A. Zaim, M. Kerouad, J. Supercond. Nov. Magn. 29, 971 (2016).
26. D.C. da Silva, A.S. de Arruda, M. Godoy, Int. J. Mod. Phys. C 31, 2050124 (2020).
27. D. Lv, W. Wang, J.P. Liu, D.Q. Guo, S.X. Li, J. Magn. Magn. Mater. 465, 348 (2018).
28. O. Dakir, A. El Kenz, A. Benyoussef, Physica A 426, 45 (2015).
29. J. Strečka, Physica A 360, 379 (2006).
30. W. Wang, Y. Liu, Z-Y. Gao, X-R. Zhao, Y. Yang, S. Yang, Physica E 101, 110 (2018).
31. T. Kaneyoshi, Physica A 390, 3697 (2011).
32. M. Boughrara, M. Kerouad, A. Zaim, J. Magn. Magn. Mater. 368, 169 (2014).
33. B. Boughazi, M. Boughrara, M. Kerouad, Physica A 465, 628 (2017).
34. D. Lv, F. Wang, R-J. Liu, Q. Xue, S-X. Li, J. Alloys Compd. 701, 935 (2017).
35. N. Hachem, I.A. Badrour, A. El Antari, A. Lafhal, M. Madani, M. El Bouziani, Chin. J. Phys. 71, 12 (2021).
36. N. Hachem, M. El Bouziani, SPIN 12, 2250025 (2022).